Loss Minimization Method Based on Three-Phase Asymmetric Control for Doubly Salient Electromagnetic Generation Systems

Guilu Min, *Student Member, IEEE*, Yanwu Xu, *Member, IEEE*, Shuye Ding, and Zhuoran Zhang, *Senior Member, IEEE*

***Abstract*—A loss minimization method based on three-phase asymmetric control is proposed for doubly salient electromagnetic generator (DSEG) systems. The three-phase magnetic circuit of DSEG is asymmetrical because of the parallel structure of the stator poles. The DSEG has the problems of uneven flux density distribution and partial oversaturation. Iron losses are not uniformly distributed in the core and difficult to analyze and calculate. According to the load resistance and conduction angle, the fundamental and harmonic distribution characteristics of the flux density of the core are obtained, and accurate iron loss calculation is realized. The three-phase armature currents in DSEG are also asymmetrical in the armature windings, so the copper losses are not uniformly distributed. In addition, the loss composition of DESG is analyzed, and an online method to calculate copper and iron losses is proposed. The three-phase asymmetric control method is implemented with the copper and iron loss models, and the optimum conduction angle and optimum asymmetric conduction angle are determined through the perturbation observation method. The proposed method is proven to be effective through experiments.**

***Index Terms*—Active rectifier, doubly salient electromagnetic generator (DSEG), iron loss model, loss calculation, three-phase asymmetric control.**

I. Introduction

THE doubly salient electromagnetic generator (DSEG) has no windings on the rotor and possesses a simple structure, robustness, and reliability [1]. The inclusion of the field winding, which results in flexible field regulation capability, gives this generator another advantage over permanent magnet motors [2]. Doubly salient machines have been applied in wind power generation systems and in aircraft applications [3]. However, the existence of the field winding reduces the efficiency of DSEG. Therefore, DSEG losses must be calculated and analyzed to improve efficiency.

Extensive research has been conducted on efficiency optimization control for asynchronous and permanent magnet/hybrid excitation synchronous motors. A loss minimization control method for wound-rotor synchronous machines was proposed in [4] to address severe heating in armature windings due to excessive current. In this method, the controllable electrical loss function is derived by simplifying the equivalent circuits and considering the time derivative of the field current. Then, the optimum d-axis current for minimizing losses is determined.

Overload conditions in asynchronous motors significantly affect electromagnetic parameters and losses. The impact of overloading on electromagnetic parameters and loss characteristics was comprehensively analyzed in [5]. Loss distributions in copper and iron were determined using advanced loss calculation models, incorporating the effects of skin effect and magnetic saturation. An optimized current control method was proposed for hybrid excitation motors [6]. This method ensures that torque and speed requirements are met with minimal copper consumption by extending the Lagrange multiplier optimization algorithm. Nevertheless, these models cannot be applied to DSEG systems due to structural differences.

In [7], the effect of material magnetic properties on motor efficiency and iron losses in a switched reluctance machine (SRM) was investigated with various non-oriented steels as the core materials. Different parts of SRM exhibit different magnetic flux density. Thus, iron losses were estimated with distinct equations based on flux density waveform classification. Although this method improves accuracy, it depends on empirical data and lacks general applicability. Current efficiency optimization techniques focus on two main areas: loss model control [8] and search techniques [9]. Iron losses, a significant component of overall losses, substantially impact efficiency and dynamic performance metrics. In [10], a dynamic simulation model of SRM was developed by considering the iron loss and interphase mutual inductance of the motor, and favorable results were obtained. A nonlinear lumped-parameter model was proposed to analyze SRM iron losses [11]. In [12], the iron losses are equated to eddy current loss resistance and hysteresis loss resistance. In addition, the model derives the variation of iron loss with respect to time. Nevertheless, the methods proposed in [11]

Received 15 February 2025; revised 10 June 2025 and 13 August 2025; accepted 27 September 2025. Date of publication 2 October 2025; date of current version 13 November 2025. This work was supported in part by the National Natural Science Foundation of China under Grant 52377060 and Grant 52407055 and in part by the Major Science and Technology Projects in Jiangsu Province under Grant BG2024039. Recommended for publication by Associate Editor F. Freijedo. *(Corresponding authors: Yanwu Xu; Shuye Ding.)*

Guilu Min, Yanwu Xu, and Shuye Ding are with the School of Electrical and Automation Engineering, Nanjing Normal University (NNU), Nanjing 210000, China (e-mail: 221802021@njnu.edu.cn; xuyanwu1990@163.com; 61211@njnu.edu.cn).

Zhuoran Zhang is with the Center for More-Electric-Aircraft Power System, Nanjing University of Aeronautics and Astronautics, Nanjing 211106, China (e-mail: apsc-zzr@nuaa.edu.cn).

Color versions of one or more figures in this article are available at https://doi.org/10.1109/TPEL.2025.3617106.

Digital Object Identifier 10.1109/TPEL.2025.3617106

and [12] require extensive experiments to determine the relevant parameters in the nonlinear parametric model.

In [13], a three-phase nine-state control method for DSEG systems was introduced. The relationship between conduction angle and phase current was systematically analyzed. Additionally, the influence of conduction angles on phase current variations was described in detail. Meanwhile, self-tuning control of advance angles was proposed based on advanced angle control in [14]. The appropriate advance angle was selected to improve the output torque and compensate for the imbalance of the three-phase current waveform. DSEG was divided into eight sections, and the flux density of each section was analyzed in detail [15]. An iron loss model was developed by examining the magnetic field distribution. On the basis of the variation rule of flux density, a core-loss coefficient determination method was proposed in [16], and the model for calculating the core loss under high-speed DSEG operation was improved. Meanwhile, in [17], the characteristics of hollow conductor ac losses were analyzed, and an AC loss model was established to quickly calculate the ac losses of different structures. However, the aforementioned methods are optimized from the DSEG design perspective.

On the basis of angular position control (APC), conduction angles were connected to a copper loss optimal conduction angle trajectory in [18]. The loss of DSEG mainly included copper, iron, friction, and wind age losses. However, it targets low-speed, high-load conditions and ignores other losses. In [19], the losses of a DSEG system based on APC were studied, including variation trends. An efficiency optimization control method based on APC (EOAPC) with the Bayesian optimization–random forest model was proposed. EOAPC is based on the iron loss model to select the conduction angle that minimized the integrated loss. Though various losses were analyzed, magnetic flux density was not studied in detail. Artificial intelligence algorithms and extensive simulations were used, but the three-phase imbalance caused by parallel poles was ignored. Therefore, the calculation model lacks accuracy.

A loss minimization method with asymmetric control is proposed for the DSEG system based on an active rectifier. The iron loss model is optimized based on flux density distribution. The iron losses of the fundamental and harmonic components are calculated separately. In addition, copper and iron loss compositions are analyzed in detail. Accordingly, a three-phase asymmetric control method is implemented. Experiments were conducted on the DSEG system to validate the effectiveness of the proposed method. The main contributions are summarized as follows.

1) Accurate iron loss calculation model based on the effects of load resistance and conduction angle on magnetic flux density.
2) Considering the asymmetric three-phase structure of DSEG and its uneven loss distribution, a loss model is proposed and its accuracy is experimentally verified.
3) The optimal control of efficiency is realized based on the loss model, and the optimal conduction angle and asymmetric conduction angle are determined by the perturbation observation method. Compared with the existing loss optimization methods, the proposed method can improve the efficiency of the DSEG system more effectively.

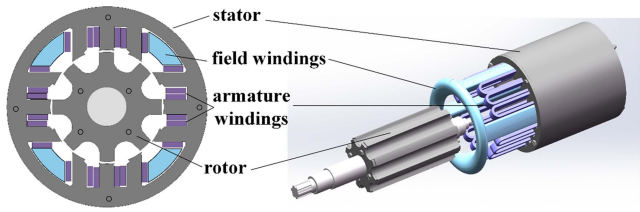

Fig. 1. Structure and cross section of the DSEG.

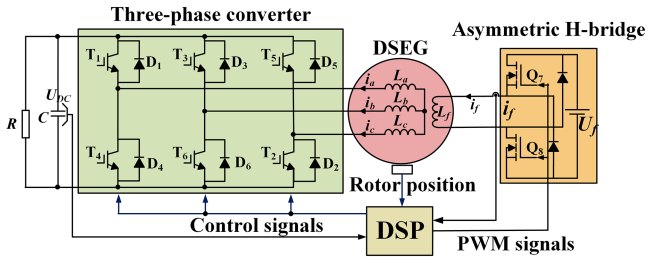

Fig. 2. DSEG systems with active rectifier.

The rest of this article is organized as follows. In Section II, the control methods of DSEG are analyzed and compared, and the loss components of DSEG are analyzed in detail. A model for calculating iron loss is developed based on the flux density characteristics. In Section III, a DSEG loss optimization method based on three-phase asymmetric control is proposed. In Section IV, experiments are performed to verify the performance of the proposed method. Finally, Section V concludes this article.

II. Control Methods for DSEG Systems

The structure and cross section of three-phase 12-/8-pole DSEG are illustrated in Fig. 1. The stator and rotor have a salient pole structure, and the rotor has no windings and permanent magnets. The armature and field windings on the stator are concentrated windings. In DSEG, one set of field windings is shared by three stator poles. The stators have a parallel pole structure and generate two pairs of magnetic fields. Therefore, the three-phase magnetic circuit is asymmetrical. This special construction results in an uneven distribution of DSEG armature-winding and rectifier-bridge losses.

A. Active Rectifier for DSEG Systems

A conventional diode rectifier (DR) is simple to control, easy to implement, and reliable. However, DR circuits lead to low output voltage and power from DSEG. In addition, during load operation, the armature reaction reduces the amount of change in the phase flux linkage, making the external characteristics soft. As illustrated in Fig. 2, the field winding is linked to the asymmetric H-bridge. The armature winding is linked to the three-phase converter. Output power is attained by regulating the conduction state of the three-phase converter switches. The active rectifier controls the switches appropriately, allowing the

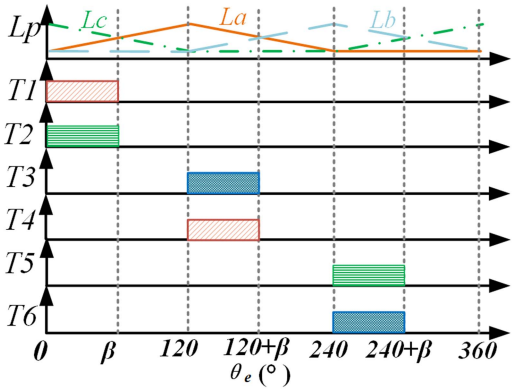

Fig. 3. Conduction logic of APC and corresponding inductance waveforms.

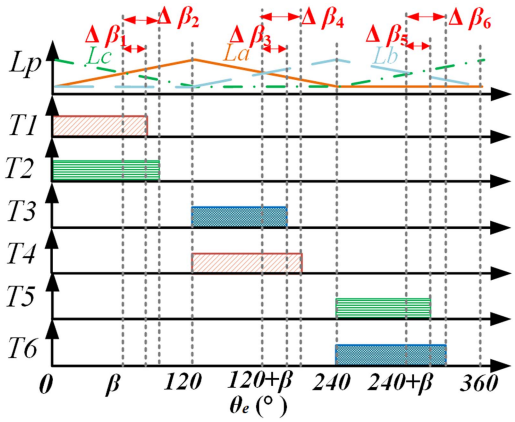

Fig. 4. Conduction logic of asymmetric control and corresponding inductance waveforms.

armature current to vary within corresponding intervals. As a result, the negative effect of phase change is reduced, and the output power increases. Active rectifier control methods for DSEG systems mainly include APC and pulse width modulation control. In DSEG systems, high output voltage and power are obtained with APC method.

In DSEG, flux linkage ψ can be expressed as

$$\begin{bmatrix}\psi_a\\ \psi_b\\ \psi_c\\ \psi_f\end{bmatrix}=\begin{bmatrix}L_a & L_{ab} & L_{ac} & L_{af}\\ L_{ba} & L_b & L_{bc} & L_{bf}\\ L_{ca} & L_{cb} & L_c & L_{cf}\\ L_{fa} & L_{fb} & L_{fc} & L_f\end{bmatrix}\begin{bmatrix}i_a\\ i_b\\ i_c\\ i_f\end{bmatrix} \tag{1}$$

where L_x is the self-inductance of the x-phase windings, L_{xy} is the mutual inductance between windings, i_p is the p-phase armature current, and i_f is the field current. Given the special structure of DSEG, the armature and field windings are highly coupled. Therefore, the mutual inductance of the field and armature windings is large. The mutual inductance of the three-phase windings is small and negligible.

Fig. 3 illustrates the conduction logic of APC and the corresponding inductance waveforms. L_x can be divided into three equal-width parts in each electrical cycle of the simplified model of DSEG. With Phase A as an example, when L_a is in the ascending interval, the insulated-gate bipolar transistor (IGBT) attached to the upper bridge arm is turned ON for $\beta°$. When L_a is in the descending interval, the IGBT attached to the lower bridge arm is turned ON for $\beta°$. When L_a is in the constant interval, IGBT is turned OFF. The APC method enhances the output power by increasing the armature current.

B. Three-phase Asymmetric Control

Due to the inherent structural characteristics of the DSEG, the loss distribution among the three-phase windings tends to be uneven. This uneven distribution may lead to localized core saturation, excessive temperature rise, and a reduction in system reliability. To address this issue, a three-phase asymmetric control method is introduced by independently adjusting the conduction angles of the IGBTs in each phase.

Fig. 4 illustrates the conduction logic diagram under the proposed three-phase asymmetric control strategy. Unlike conventional methods, this method introduces phase-specific conduction angles (denoted as $\Delta\beta_1$ to $\Delta\beta_6$). By customizing the conduction timing based on the individual magnetic field and current characteristics of each phase, the loss distribution among the windings can be effectively optimized. This will reduce localized magnetic saturation and lower phase current stresses. Consequently, the operational efficiency and reliability of the DSEG system are significantly enhanced.

Fig. 5 illustrates the conduction mode diagrams for the L_a ascending interval. The commutation process occurring during the inductance falling stage weakens the energy conversion capability of the system and increases overall losses [20]. In Fig. 5(a), T_1 and T_2 are turned ON, and current passes through phases A and C. In Fig. 5(b), T_1 is turned OFF in advance. Turning OFF the upper- arm IGBT reduces negative current amplitude, which in turn decreases the current commutation zone. The efficiency of the DSEG system is improved by three-phase asymmetric control.

III. Loss Minimization Model

The DSEG loss is mainly composed of copper loss P_{Cu}, iron loss P_{Fe}, mechanical loss P_m, and stray loss P_Δ. P_m is generated by friction from the bearings, wind resistance, and other factors. P_Δ and P_m are mainly affected by operation speed n. From the control perspective, no other measures can further reduce DSEG loss. Therefore, mechanical and stray losses do not need to be included in the loss model. Efficiency is improved mainly through asymmetric control, thereby reducing copper and iron losses.

A. Analysis of Iron Losses in the DSEG System

Iron loss consists of hysteresis loss P_h, eddy-current loss P_c, and excess loss P_e in [21]. In accordance with Bertotti's iron loss model, P_{Fe} can be presented as

$$\begin{aligned}P_{Fe}&=P_h+P_c+P_e\\&=k_hfB^2+k_cf^2B^2+k_ef^{1.5}B^{1.5},\end{aligned} \tag{2}$$

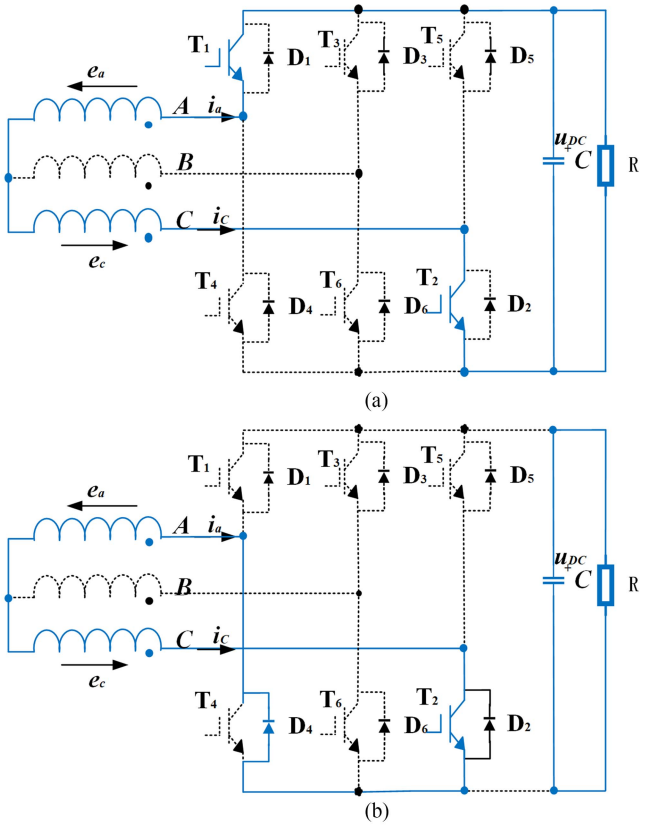

Fig. 5. Three-phase asymmetric conduction mode. (a) T_1 and T_2 are turned ON. (b) T_1 is turned ON, T_2 is turned OFF).

where k_h, k_c, and k_e are the coefficients of hysteresis, eddy-current, and excess losses, respectively, and B and f are the amplitude and frequency of flux density, respectively. Given that the flux density waveform of the DSEG system is not sinusoidal. Therefore (2) does not apply to the DSEG system. Therefore, the flux density waveform is expanded in the Fourier series, and the nonsinusoidal waveform is expanded as a sum of fundamental and multiple harmonics. The iron loss model is calculated separately for fundamental and harmonic iron losses. A-phase flux linkage ψ_a in the DSEG system can be presented as follows:

$$\psi_a = N\phi_a = NSB_a = L_{af}i_f + L_a i_a \tag{3}$$

where N is the number of turns of windings, ψ_x is x-phase magnetic flux, B_x is x-phase flux density in the stator core, and S is the cross-sectional area. i_a can be presented as

$$i_a = \frac{e_a - e_b}{R} \tag{4}$$

where e_x is the x-phase back-EMF, and R is the load resistance. Introducing (4) into (3) yields

$$\mathrm{NSB}_a = L_{af}i_f + L_a\frac{e_a - e_b}{2R}. \tag{5}$$

e_x can be presented as

$$e_a = \frac{d\psi}{dt} = NS\frac{dB_a}{dt}. \tag{6}$$

In the DSEG system

$$\frac{dB_a}{dt} = -\frac{dB_b}{dt}. \tag{7}$$

Introducing (6) and (7) into (5) yields

$$NSB_a = L_{af}i_f + \frac{L_a NS}{2R}\cdot\frac{dB_a}{dt}. \tag{8}$$

After solving differential (8), B_a can be presented as

$$B_a(t) = C\cdot e^{\left(-\frac{2Rt}{L_a(\theta(t))}\right)} + \frac{L_{af}(\theta(t))\cdot i_f}{NS} \tag{9}$$

where C is a constant. To simplify the calculation, it is idealized that the inductance varies linearly, and L_{af} can be expressed as

$$L_{af}(\theta) = \begin{cases} k\theta + b, & 0^\circ \le \theta < 120^\circ \\ -k\theta + 240k + b, & 120^\circ \le \theta < 240^\circ \\ b, & 40^\circ \le \theta < 360^\circ \end{cases}. \tag{10}$$

B_a consists of B_{a1} and B_{a2}

$$\begin{aligned} B_a(t) &= B_{a1}(t) + B_{a2}(t) \\ B_{a1}(t) &= \frac{L_{af}(\theta(t))\cdot i_f}{NS} \\ B_{a2}(t) &= C\cdot e^{\left(-\frac{2Rt}{L_a(\theta(t))}\right)}. \end{aligned} \tag{11}$$

A Fourier decomposition is performed on B_a

$$\begin{aligned} B_a(t) &= \frac{a_0}{2} + \sum_{n=1}^{\infty}\left[a_n\cos(n\omega_e t) + b_n\sin(n\omega_e t)\right] \\ a_n &= \frac{2}{T}\int_0^T B_a(t)\cos(n\omega_e t)dt \\ b_n &= \frac{2}{T}\int_0^T B_a(t)\sin(n\omega_e t)dt \end{aligned} \tag{12}$$

where ω_e is the angular velocity of the fundamental frequency; a_n and b_n are the Fourier coefficients representing the amplitudes of the cosine and sine terms, respectively; B_n is the amplitude of the n-th harmonic, which can be expressed as

$$B_n = \sqrt{a_n^2 + b_n^2}. \tag{13}$$

The analyses are performed separately for B_{a1} and B_{a2}. For B_{a1}, $L_{af}(\theta)$ is a periodic function and can be represented by Fourier decomposition as follows:

$$L_{af}(\theta(t)) = \sum_{n=0}^{\infty} K_n\cos(n\omega_e t + \phi_n) \tag{14}$$

where K_n is the amplitude of L_{af} 's nth harmonic, ϕ_n is the phase angle of L_{af} 's nth harmonic

$$B_{a1}(t) = \frac{i_f}{NS}\sum_{n=0}^{\infty} K_n\cos(n\omega_e t + \phi_n). \tag{15}$$

The amplitudes of the fundamental and harmonic components of B_{a1} are positively correlated with i_f.

B_{a2} can be approximately equivalently expressed as

$$B_{a2}(t) \approx C\cdot e^{\left(-\frac{2R}{<L_a>}t\right)} \tag{16}$$

where, $\langle L_a \rangle$ is the average value of L_a (θ). Applying the Fourier transform to B_{a2} yields

$$\mathcal{F}\{B_{a2}\} = C \cdot \frac{2R/ < L_a >}{(2R/ < L_a >)^2 + (2\pi f_n)^2} \tag{17}$$

where f_n is the frequency of the *n*th harmonic.

Since L_a is small

$$\frac{2R}{< L_a >} \gg 2\pi f_n. \tag{18}$$

Accordingly, the amplitude of the *n*th harmonic of B_{a2} is positively correlated with 1/*R*

$$B_n^{a2} \propto \frac{2R/ < L_a >}{(2R/ < L_a >)^2} = \frac{< L_a >}{2R}$$

$$B_n^{a2} \propto \frac{1}{R} \tag{19}$$

where B_n^{a2} is the *n*th harmonic of B_{a2}.

Based on the above analysis, the amplitude of the *n*th harmonic of B_{a1} is

$$B_n^{a1} = \frac{i_f}{NS} K_n. \tag{20}$$

The amplitude of the *n*th harmonic of B_{a2} is

$$B_n^{a2} = \frac{C}{\sqrt{(2R/ < L_a >)^2 + (2\pi f_n)^2}}. \tag{21}$$

The total harmonic amplitude B_n^{total} can be expressed as

$$B_n^{\text{total}} = \sqrt{(B_n^{a1})^2 + (B_n^{a2})^2}$$

$$= \sqrt{\left(\frac{i_f K_n}{NS}\right)^2 + \left(\frac{C}{\sqrt{(2R/ < L_a >)^2 + (2\pi f_n)^2}}\right)^2}. \tag{22}$$

A conclusion that can be derived is that flux density is mainly related to field current and load resistance. *R* significantly affects the harmonic amplitude, but has little effect on the fundamental component of flux density. i_f linearly increases the fundamental and harmonic amplitudes of the flux density. The magnetic field at the core of DSEG is analyzed under different field currents. The flux density in the DSEG is mainly distributed in the stator and rotor teeth. The flux density in the stator and rotor yokes is very small and produces negligible iron losses. When the stator and rotor teeth are aligned, the flux density in the teeth can be idealized as the same. When not aligned, the flux density can be considered as zero. Since the flux density waveform is not sinusoidal, Fourier analysis is required. The nonsinusoidal waveform is expanded into a sum of the fundamental and multiple harmonics. The flux densities are obtained from no-load finite element simulations [see Fig. 6] and analyzed by Fourier transform. The fundamental amplitude of the flux density increases with the field current. Since iron loss is positively correlated with both the frequency and amplitude of the flux density, an increase in the fundamental amplitude consequently leads to higher iron losses. The flux density contains significant

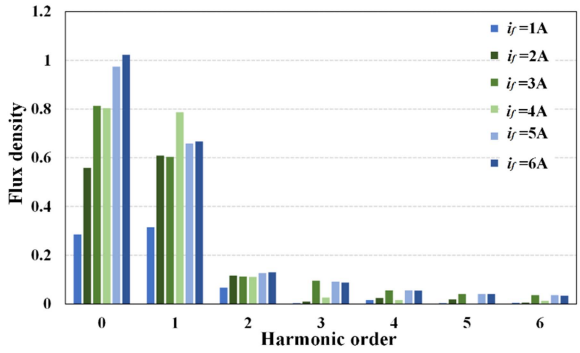

Fig. 6. Fourier transformation results for amplitudes of A-phase flux densities under no-load. ($n = 4000$ r/min).

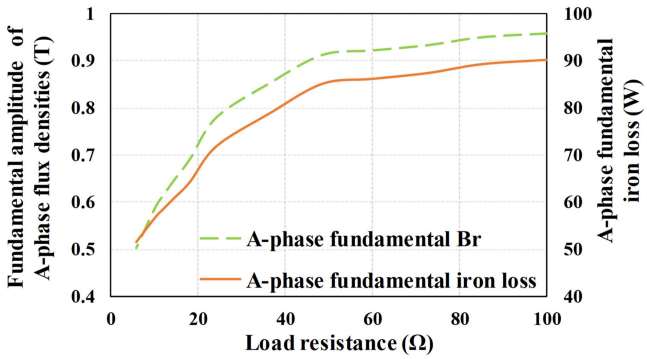

Fig. 7. Fundamental amplitude of the flux density and iron loss under different load resistances for the DSEG system. ($i_f = 3$ A).

harmonic components, especially under high field current conditions. The fundamental component dominates, while harmonics component still contributes notably to flux density, indicating the necessity of considering harmonic losses in iron loss evaluation. The iron losses incurred at different frequencies are given as

$$P_{Fe-\text{density}} = \sum_{n=1}^{N} \left(k_h f_n B_n^2 + k_c f_n^2 B_n^2 + k_e f_n^{1.5} B_n^{1.5}\right) \tag{23}$$

where *N* is the highest number of harmonics of Fourier transform and B_n is the magnitude of flux density at the *n*th harmonic. The fundamental amplitude of flux density is modeled and the fundamental iron loss is calculated for different load resistances, as illustrated in Fig. 7. Although the armature current has a notable influence on the fundamental amplitude of the flux density, its quantitative effect is difficult to evaluate. Therefore, the impact of load resistance on the fundamental amplitude is analyzed instead, as the relationship is more tractable and indirectly reflects the variation of armature current. The results indicate that the fundamental amplitude and the corresponding iron loss increase with higher load resistance. This model enables the estimation of the fundamental flux density amplitude under different load conditions. With (2), the corresponding fundamental iron loss can be calculated. When the load resistance approaches 80Ω, flux density approaches saturation. At this point, the fundamental amplitude increases slowly. A Fourier decomposition was

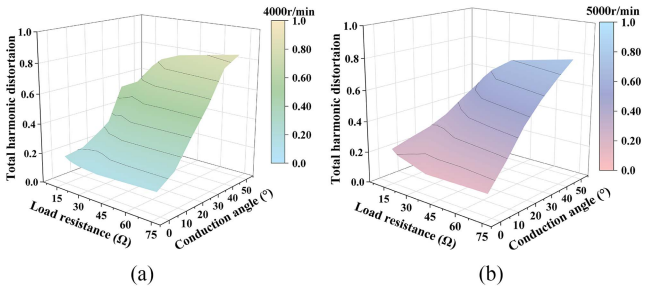

Fig. 8. Total harmonic content at different speeds. ($i_f = 3$A) (a) $n =$ 4000 r/min. (b) $n = 5000$ r/min.

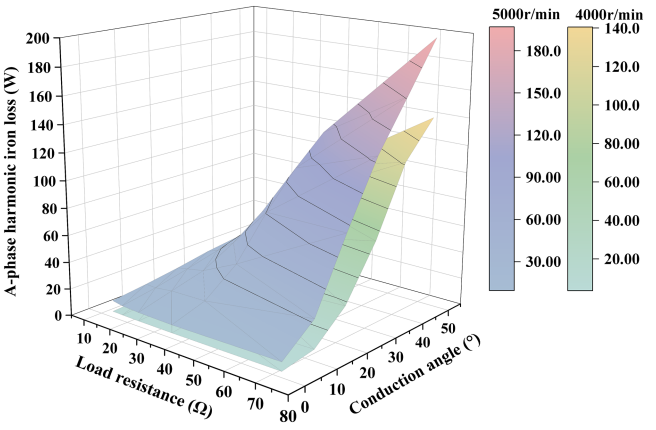

Fig. 9. Harmonic iron loss model. ($i_f = 3$ A).

performed on the flux density waveform, and the total harmonic distortion was calculated up to the eighth harmonic

$$\mathrm{THD} = \frac{\sqrt{\sum_{n=2}^{8} B_n^2}}{B_1} \tag{24}$$

where B_1 is the amplitude of the fundamental component of the flux density, B_n are the amplitudes of the second to eighth harmonic components. The analysis is carried out by analyzing the total harmonic content at different operating conditions as illustrated in Fig. 8. For the same operating conditions, the larger the conduction angle, the larger the total harmonic content.

As illustrated in Fig. 9, the harmonic iron loss model is calculated by (2). It is derived by multiplying the frequency by the corresponding multiplier and then multiplying by the harmonic value. Harmonic iron loss is proportional to the conduction angle. The higher the speed is, and the larger the harmonic iron losses are. Iron losses can be calculated with the fundamental and harmonic iron loss models.

B. Copper Loss Analysis

The copper losses in the DSEG system are mainly composed of armature-winding copper losses P_{Cu-p} and field-winding copper losses P_{Cu-f}. For the individual windings, internal resistance r_x can be obtained by measurement. Therefore, the

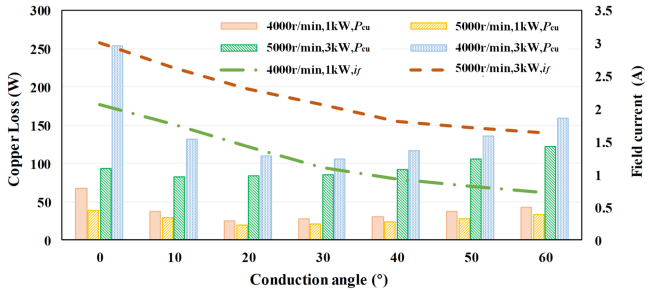

Fig. 10. Copper loss and field current under different operating conditions.

total copper loss (P_{Cu}) can be presented as

$$P_{Cu} = P_{Cu-p} + P_{Cu-f} = {i_a}^2 r_a + {i_b}^2 r_b + {i_c}^2 r_c + {i_f}^2 r_f \tag{25}$$

where i_x is the three-phase armature current. The variation in copper loss is mainly affected by the variation in armature and field currents. The armature-winding and field-winding equivalent resistances are made constant by default without considering the slight effect caused by the temperature rise.

As illustrated in Fig. 10, DSEG is simulated at 4000 and 5000 r/min, 1 and 3 kW, and different conduction angles. Compared with DR control, APC can effectively lower the field current at the same speed, load, and busbar voltage. At the same speed and conduction angle, the higher the load is, the higher the armature and field currents are, resulting in high copper losses. The lower the speed is, the higher the copper loss is for the same load. At low speeds, a high field current is required to maintain the same output power. As the conduction angle increases, armature current gradually rises, and field current gradually decreases. APC reduces the copper loss in the field winding but increases the armature-winding copper loss. The total copper loss decreases and then increases as the conduction angle increases. Under the same operating conditions, APC reduces the field current, which reduces the magnitude of the dc bias field and ultimately decreases the iron losses. Therefore, a conduction angle that minimizes the total loss exists. The use of the APC method can effectively increase the output capacity of the DSEG system.

C. Loss Minimization Method Based on Asymmetric Control

According to the analysis, the total losses tend to decrease and then increase as the conduction angle increases. Based on this observation, a loss minimization method based on three-phase asymmetric control is proposed. The technical route of the proposed control method is illustrated in Fig. 11. Based on the measured rotational speed, load resistance, field current, and three-phase armature currents, the corresponding iron losses can be obtained through the fundamental and harmonic iron loss models. The rotational speed is measured by a speed sensor and the current is measured by a current sensor. The copper loss is calculated by (25). Subsequently, the conduction angle β is incremented in 5° steps, and at each interval, the loss is recalculated based on the experimentally measured parameters. The corresponding resistances of the armature winding (r_p) and

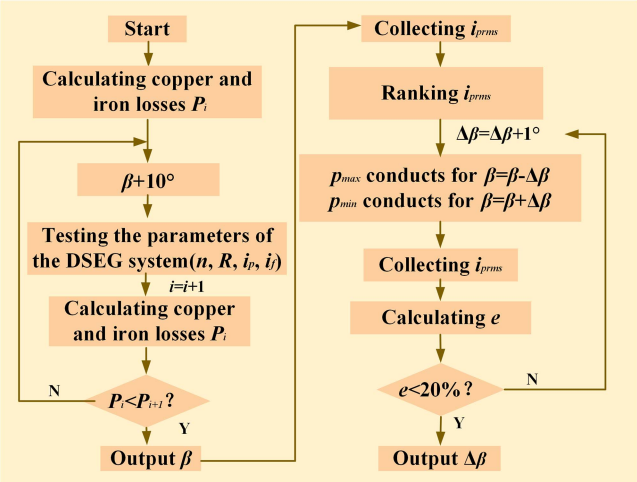

Fig. 11. Flowchart of loss minimization method based on three-phase asymmetric control.

TABLE I
PARAMETERS OF THE DSEG

Parameters	value	Parameters	value
Number of stator poles	12	Rotor core material	35WW270
Number of rotor poles	8	Rated voltage (V)	270
Speed range (r/m)	4000-8000	i_f (A)	0-6
Rated power (kW)	9	r_p (Ω)	0.1134
Stator core material	35WW270	r_f (Ω)	5.794

the field winding (r_f) are inherent parameters of the DSEG, and their values are listed in Table I. On the basis of the perturbation observation method, the optimal β and $\Delta\beta$ that minimize the loss are determined.

When $P_i > P_{i+1}$, the conduction angle continues to increase. When $P_i < P_{i+1}$, the loop terminates, and the corresponding β is outputted. The root-mean-square (RMS) values of the three-phase armature currents, i_{prms}, at this conduction angle are calculated separately. $i_{a\text{rms}}$, $i_{b\text{rms}}$, and $i_{c\text{rms}}$ are arranged in order. The phase with the largest RMS armature current is defined as $p_{\max}$, and the phase with the lowest RMS armature current is defined as $p_{\min}$. $\Delta\beta$ starts at 0° and increases by 1° per cycle. The $p_{\max}$-phase IGBTs conduct for β+$\Delta\beta$. The $p_{\min}$-phase IGBTs conduct for β-$\Delta\beta$. The RMS of the three-phase armature currents and mean square error e are calculated

$$e = \frac{\sum_{i=1}^{n} \left(i_{\text{prms}} - i_{\text{rmsmid}}\right)^2}{3} \tag{26}$$

where i_{rmsmid} is the median of the RMS value of the three-phase armature current. $\Delta\beta$ should be further increased if e exceeds 20% . $\Delta\beta$ will be outputted if e is less than 20% . If $i_{a\text{rms}} > i_{b\text{rms}} > i_{c\text{rms}}$, the conduction angles of phases A and C must be changed. $i_{a\text{rms}}$ is presented as $i_{b\text{rms}} + m$, and $i_{c\text{rms}}$ is expressed as $i_{b\text{rms}}$-n. Therefore, the total copper loss under APC can be given as

$$\begin{aligned} P_{\text{Cu-APC}} &= (i_{b\text{rms}}+m)^2 r_a + {i_{b\text{rms}}}^2 r_b + (i_{b\text{rms}}-n)^2 r_c + {i_f}^2 r_f \\ &= \left({i_{b\text{rms}}}^2 r_a + {i_{b\text{rms}}}^2 r_b + {i_{b\text{rms}}}^2 r_c + {i_f}^2 r_f\right) \\ &\quad + (2m i_{b\text{rms}} + m^2) r_a + (-2n i_{b\text{rms}} + n^2) r_c \end{aligned} \tag{27}$$

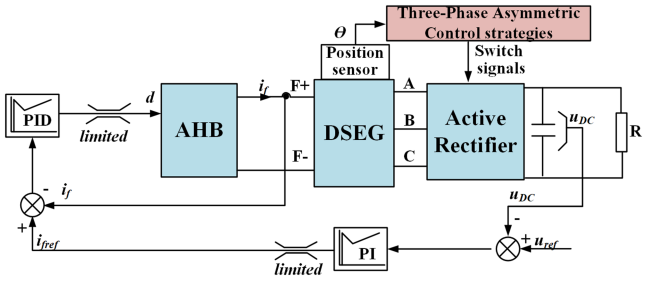

Fig. 12. Control scheme of the proposed method.

With three-phase asymmetric control, $i_{a\text{rms}}$ and $i_{c\text{rms}}$ can be approximately equal to those of phase B. Given that the average value of the three-phase armature current RMS does not change considerably, i_f is almost constant. Therefore, copper loss $P_{\text{cu-AC}}$ under asymmetric control can be presented as

$$P_{\text{Cu-AC}} = {i_{b\text{rms}}}^2 r_a + {i_{b\text{rms}}}^2 r_b + {i_{b\text{rms}}}^2 r_c + {i_f}^2 r_f. \tag{28}$$

Equation (27) indicates that $(2m i_{b\text{rms}} + m^2) r_a + (-2n i_{b\text{rms}} + n^2) r_c > 0$. Therefore, by using (27) and (28), we can prove that $P_{\text{Cu-APC}} > P_{\text{cu-AC}}$. Three-phase asymmetric control helps balance the armature currents, which effectively reduces copper losses. In addition, three-phase asymmetric control can slightly decrease the field current. Three-phase asymmetric control has no effect on the load resistance, and the variation in conduction angle can also be neglected. Therefore, this control strategy slightly reduces the fundamental iron loss while having minimal impact on the harmonic iron loss. As a result, the overall iron loss can be reduced under three-phase asymmetric control. This minimizes total losses and avoids overloading single-phase windings. Fig. 12 is a block diagram of the control strategy for a DSEG system. The field current is controlled by voltage outer loop proportional integral controller and current inner loop proportional integral derivative controller. The purpose is to fix the bus voltage at 270 V. Parameters, such as speed, load, armature current, busbar voltage, field current are collected through sensors so as to calculate the losses according to the loss model. The β and $\Delta\beta$ are optimized online via perturbation observation method to derive the optimal conduction angle for three-phase asymmetric control.

IV. EXPERIMENTAL VALIDATION

As illustrated in Fig. 13, an experimental platform is built to validate the proposed loss minimization method with three-phase asymmetric control. The parameters of the DSEG are given in Table I. A torque transducer is installed in the experimental platform so that the input power can be calculated. The armature winding is connected to the three-phase full- bridge rectifier. Active rectifier control and DR control are realized with the three-phase full-bridge rectifier. The three-phase currents are collected by current sensors, and the field current is generated by a dc power source. The magnitude of the field current is controlled by the asymmetric H-bridge, and the field current is collected by a current sensor. In addition, closed-loop control of the output voltage is realized using this experimental platform. Busbar voltage is maintained at 270 V. The computer

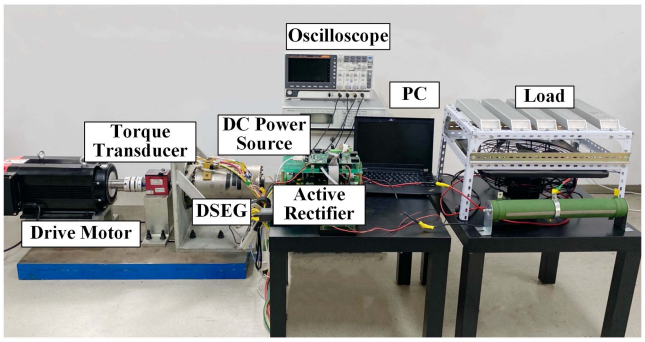

Fig. 13. Experimental platform.

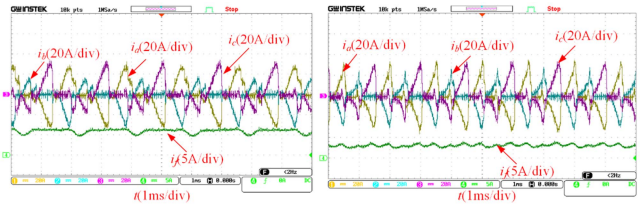

Fig. 14. Phase currents, field current with a diode rectifier (3 kW load). (a) n = 4000r/min. (b) n = 5000 r/min.

communicates with the digital signal processor in real time to achieve loss-minimizing control of the conduction angle. Different working conditions are set, parameters are gathered, and efficiency is calculated.

In the experiment, several common operating conditions were chosen to verify the validity of the proposed method. The conventional method and the proposed method are examined within the range of 4000–5000 r/min. DR control, EOAPC, and three-phase asymmetric control are compared experimentally. The input power of DSEG, P_1, can be presented as

$$P_1 = T\omega = \frac{Tn}{9550 \times 10^3} \tag{29}$$

where ω is the rotor angular speed and n and T are the speed and torque on the shaft, respectively. The input power of the whole DSEG system, P_{in}, is the sum of DSEG input power P_1 and field current power P_f. Thus, efficiency η can be presented as

$$\eta = \frac{P_2}{P_1 + P_f} \tag{30}$$

where P_2 is the output power of the DSEG system.

The experimental waveforms and corresponding conditions of the DSEG system at a constant speed of 4000 r/min are presented in Figs. 14–18 and Table II. The control methods are compared, including the DR control method, EOAPC method, and the proposed method. Two load conditions, 24.3 and 18.225 Ω, were tested. The optimal conduction angle, and its compensation value $\Delta\beta$ were adjusted for the proposed method to optimize performance. Table III gives the corresponding efficiency and current data under the same operating condition. Compared

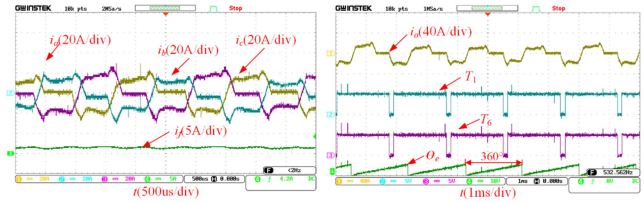

Fig. 15. Armature currents, field current, and control signals with EOAPC (n = 4000 r/min, 3 kW load, $\beta = 30°$).

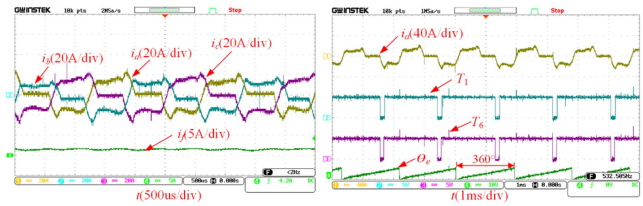

Fig. 16. Armature currents, field current, and control signals with three-phase asymmetric control (n = 4000 r/min, 3kW load, $\beta = 30°$, $\Delta\beta = 5°$).

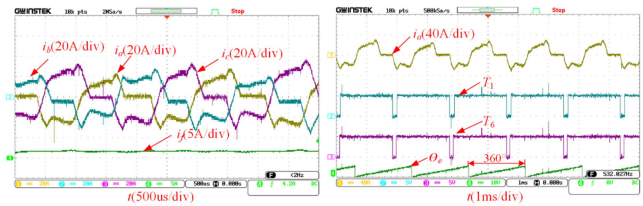

Fig. 17. Armature currents, field current, and control signals with EOAPC (n = 4000 r/min, 4 kW load, $\beta = 35°$).

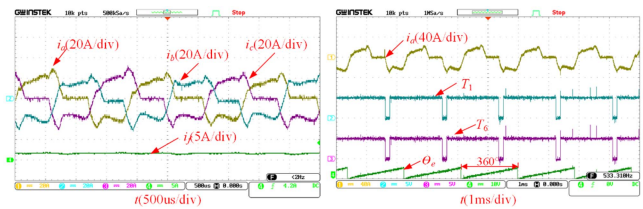

Fig. 18. Armature currents, field current, and control signals with three-phase asymmetric control (n = 4000 r/min, 4kW load, $\beta = 35°$, $\Delta\beta = 3°$).

with the DR and EOAPC, the proposed method achieves higher efficiency, reaching 90% and 92% under the two load conditions.

Fig. 14(b), along with Figs. 19–22 and Table IV present the experimental results of the DSEG system at a constant speed of 5000 r/min under different control methods. Compared with the DR, both EOAPC and the proposed method improve efficiency and current balance. The corresponding efficiency and current data for the same operating conditions are presented in Table V. Notably, the proposed method achieves higher efficiency (up to 91%) and more uniform armature currents, especially under heavy-load conditions.

In the experiment, the iron loss was obtained indirectly by subtracting the measured copper loss and mechanical loss from the total loss. The total loss is obtained by subtracting the output

TABLE II
EXPERIMENTAL CONDITIONS OF THE DSEG SYSTEM ($N = 4000$ R/MIN)

Figure number	Control method	Speed (r/min)	Load (Ω)	i_f(A)	β (°)	$\Delta\beta$ (°)
Fig. 14 (a)	DR	4000	24.3	5.9	0	0
Fig. 15	EOAPC	4000	24.3	1.39	30	0
Fig. 16	Proposed method	4000	24.3	1.38	30	8
Fig. 17	EOAPC	4000	18.225	1.58	35	0
Fig. 18	Proposed method	4000	18.225	1.58	35	3

TABLE III
EFFICIENCY OF THE DSEG SYSTEM ($N = 4000$ R/MIN)

Figure number	Input power (kW)	Output power (kW)	η (%)	i_{arms} (A)	i_{brms} (A)	i_{crms} (A)
Fig. 14(a)	3.551	3.0	86	14.5	9.48	12.5
Fig. 15	3.409	3.0	88	12.7	12.1	14.3
Fig. 16	3.334	3.0	90	12.5	12.8	12.8
Fig. 17	4.546	4.0	90	15.8	14.7	17.8
Fig. 18	4.396	4.0	92	15.7	16.1	16.0

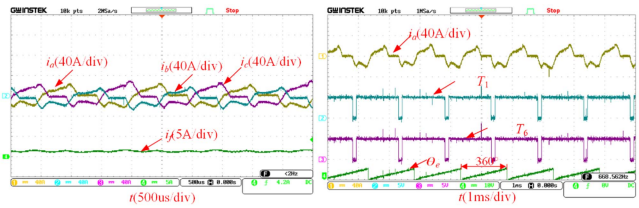

Fig. 19. Armature currents, field current, and control signals with EOAPC ($n = 5000$ r/min, 3 kW load, $\beta = 25°$).

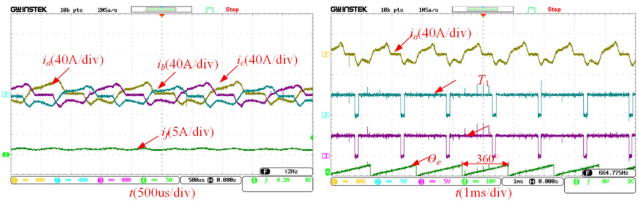

Fig. 20. Armature currents, field current, and control signals with three-phase asymmetric control ($n = 5000$ r/min, 3 kW load, $\beta = 25°$, $\Delta\beta = 5°$).

power from the total input power of the DSEG system. The copper loss was calculated based on the measured armature current and winding resistance, while the mechanical loss was estimated through no-load testing.

Fig. 23 illustrates the comparison between the iron losses calculated with the proposed iron loss model and the experimentally derived iron losses at different conduction angles. Both curves show a clear decreasing trend as the conduction angle increases. In addition, the calculated and experimental results agree very well over the whole range, proving the validity and accuracy of the proposed model. The model can be used for online iron loss estimation and provides a theoretical basis for loss minimization control in DSEG systems.

As illustrated in Fig. 24, the efficiency obtained by the different control methods is compared. The histograms are zoomed in

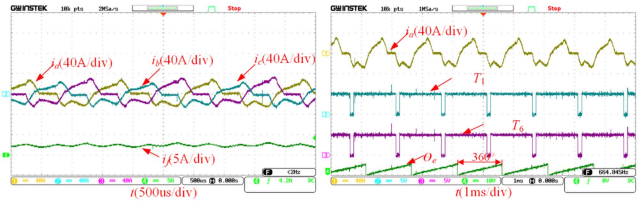

Fig. 21. Armature currents, field current, and control signals with EOAPC ($n = 5000$ r/min, 4 kW load, $\beta = 40°$).

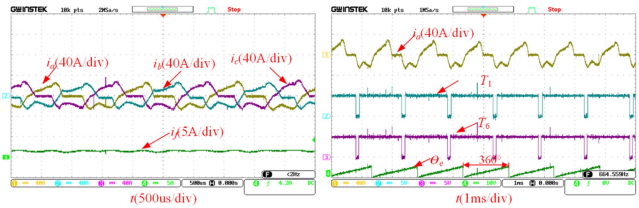

Fig. 22. Armature currents, field current, and control signals with three-phase asymmetric control ($n = 5000$ r/min, 4 kW load, $\beta = 40°$, $\Delta\beta = 8°$).

TABLE IV
EXPERIMENTAL CONDITIONS OF THE DSEG SYSTEM ($N = 5000$ R/MIN)

Figure number	Control method	Speed (r/min)	Load (Ω)	i_f(A)	β (°)	$\Delta\beta$ (°)
Fig. 14(b)	DR	5000	24.3	3	0	0
Fig. 19	EOAPC	5000	24.3	1.28	25	0
Fig. 20	Proposed method	5000	24.3	1.27	25	5
Fig. 21	EOAPC	5000	18.225	1.47	40	0
Fig. 22	Proposed method	5000	18.225	1.45	40	8

TABLE V
EFFICIENCY OF THE DSEG SYSTEM (N = 5000R/MIN)

Figure number	Input power (kW)	Output power (kW)	η (%)	i_{arms} (A)	i_{brms} (A)	i_{crms} (A)
Fig. 14(b)	3.489	3.0	86	14.4	10.8	12.3
Fig. 19	3.409	3.0	88	12.4	11.7	13.0
Fig. 20	3.371	3.0	89	12.4	12.2	12.3
Fig. 21	4.4948	4.0	89	16.9	15.3	17.8
Fig. 22	4.396	4.0	91	16.1	15.8	16.0

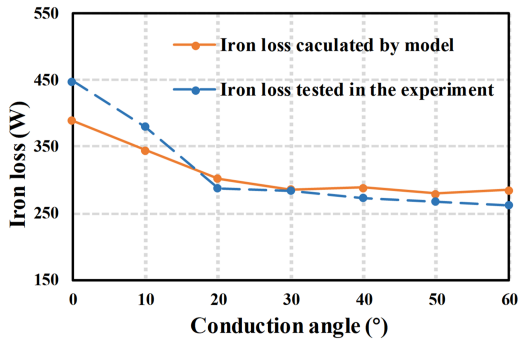

Fig. 23. Comparison of iron loss model calculation results and experimental results ($n = 5000$ r/min).

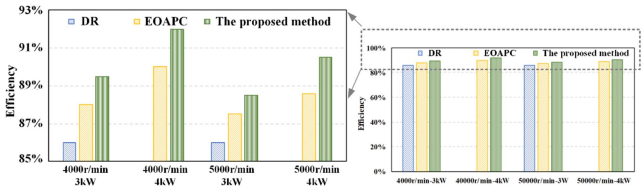

Fig. 24. Comparison of efficiency of different control methods.

for efficiencies between 85% and 93% . Compared with DR control, efficiency optimization control method based on APC, the proposed method can effectively improve the efficiency of the DSEG system, reduce the field current, and improve the ability to carry loads. Three-phase asymmetric control that determines the optimal conduction angle by the perturbation observation method can further reduce the loss of the DSEG system. The proposed method is effective in improving the efficiency by more than 1% over efficiency optimization control method based on APC under different operating conditions.

V. Conclusion

The loss minimization method based on three-phase asymmetric control is proposed for the DSEG power generation system. The three-phase magnetic circuit of DSEG is asymmetric due to the parallel structure of the stator poles. The DSEG suffers from uneven flux density distribution and partial oversaturation. The iron loss is unevenly distributed in the core, which is difficult to analyze and calculate. Comparing with the existing control methods, this article fully considers this three-phase uneven distribution problem. Furthermore, this article introduces a new approach to calculating iron loss, which is based on the study of the flux density distribution of the DSEG iron core. The accuracy of iron loss calculation is verified. Loss minimization control is achieved by a computational model based on iron and copper losses. The optimal conduction angle and the optimal asymmetric conduction angle are determined by the perturbation observation method. It is experimentally verified that the efficiency of three-phase asymmetric control is higher than that of efficiency optimization control method based on APC. In the future, the loss analysis process will be further refined by combining temperature analysis and the magnetic field behavior inside the motor core. The loss calculation accuracy and optimization results will be further improved.

References

[1] M. Cheng, K. T. Chau, and C. C. Chan, "Static characteristics of a new doubly salient permanent magnet motor," *IEEE Trans. Energy Convers.*, vol. 16, no. 1, pp. 20–25, Mar. 2001.

[2] H. Shi et al., "Copper loss optimization strategy of fault-tolerant operation for doubly salient electromagnetic generator under excitation loss," *IEEE J. Emerg. Sel. Topics Power Electron.*, vol. 12, no. 3, pp. 2626–2638, Jun. 2024.

[3] W. Zhao, M. Cheng, X. Zhu, W. Hua, and X. Kong, "Analysis of fault-tolerant performance of a doubly salient permanent-magnet motor drive using transient cosimulation method," *IEEE Trans. Ind. Electron.*, vol. 55, no. 4, pp. 1739–1748, Apr. 2008.

[4] X. Han, W. Liu, N. Jiao, P. Yao, S. Mao, and Z. Li, "Loss minimization control of aircraft wound-rotor synchronous starter–generator in the starting mode," *IEEE Trans. Power Electron.*, vol. 39, no. 5, pp. 6063–6076, May 2024.

[5] X. Qian and B. Xiong, "Research on electromagnetic parameters and loss characteristics of asynchronous motor under overload condition," in *Proc. IEEE 4th Int. Elect. Energy Conf.*, 2021, pp. 1–6.

[6] R. Mbayed, G. Salloum, L. Vido, E. Monmasson, and M. Gabsi, "Hybrid excitation synchronous motor control in electric vehicle with copper and iron losses minimization," in *Proc. 38th Annu. Conf. IEEE Ind. Electron. Soc.*, 2012, pp. 4886–4891.

[7] H. Toda, K. Senda, S. Morimoto, and T. Hiratani, "Influence of various non-oriented electrical steels on motor efficiency and iron loss in switched reluctance motor," *IEEE Trans. Magn.*, vol. 49, no. 7, pp. 3850–3853, Jul. 2013.

[8] F. Fernandez-Bernal, A. Garcia-Cerrada, and R. Faure, "Model-based loss minimization for DC and AC vector-controlled motors including core saturation," *IEEE Trans. Ind. Appl.*, vol. 36, no. 3, pp. 755–763, May/Jun. 2000.

[9] S. Vaez, V. I. John, and M. A. Rahman, "An on-line loss minimization controller for interior permanent magnet motor drives," *IEEE Trans. Energy Convers.*, vol. 14, no. 4, pp. 1435–1440, Dec. 1999.

[10] J. T. Charton et al., "Dynamic modelling of switched reluctance machines with iron losses and phase interactions," *IET Electr. Power Appl.*, vol. 153, no. 3, pp. 327–336, 2006.

[11] F. J. Perez-Cebolla, A. Martinez-Iturbe, B. Martín-del-Brío, C. Bernal, and A. Bono-Nuez, "Nonlinear lumped-circuit model for switched reluctance motors exhibiting core losses," *IEEE Trans. Ind. Electron.*, vol. 63, no. 6, pp. 3433–3445, Jun. 2016.

[12] V. Raulin, A. Radun, and I. Husain, "Modeling of losses in switched reluctance machines," *IEEE Trans. Ind. Appl.*, vol. 40, no. 6, pp. 1560–1569, Nov./Dec. 2004.

[13] L. Chen, Y. Xu, S. Ding, and Z. Zhang, "Output performance model and three-phase nine-state control for doubly salient electromagnetic generator," *IEEE Trans. Power Electron.*, vol. 38, no. 12, pp. 16022–16033, Dec. 2023.

[14] W. Jia, L. Xiao, C. Wang, and Y. Yan, "Self-tuning control of advanced angles for doubly salient motor drive system," *IEEE J. Emerg. Sel. Topics Power Electron.*, vol. 8, no. 2, pp. 1236–1247, Jun. 2020.

[15] Z. Zhang, L. Yu, L. Sun, L. Qian, and X. Huang, "Iron loss analysis of doubly salient brushless DC generators," *IEEE Trans. Ind. Electron.*, vol. 62, no. 4, pp. 2156–2163, Apr. 2015.

[16] W. Jia, L. Xiao, and D. Zhu, "Core-loss analysis of high-speed doubly salient electromagnetic machine for aeronautic starter/generator application," *IEEE Trans. Ind. Electron.*, vol. 67, no. 1, pp. 59–68, Jan. 2020.

[17] G. Hu, J. Zhang, Z. Zhang, and H. Jiang, "Analysis of loss and thermal characteristics for doubly salient electro-magnetic machine with hollow conductor," in *Proc. 26th Int. Conf. Elect. Machines Syst.*, 2023, pp. 3624–3629.

[18] Y. Xu, Z. Zhang, Z. Bian, and L. Yu, "Copper loss optimization based on bidirectional converter for doubly salient brushless starter/generator system," *IEEE Trans. Ind. Electron.*, vol. 68, no. 6, pp. 4769–4779, Jun. 2021.

[19] C. Wu, Y. Xu, Z. Zhang, and S. Ding, "Efficiency improvement method based on comprehensive loss regression model for doubly salient electromagnetic generation system," *IEEE Trans. Transp. Electrific.*, vol. 10, no. 3, pp. 7345–7357, Sep. 2024.

[20] Y. Xu, L. Xiong, B. Zhou, and K. Wang, "Asymmetric current control strategy for doubly salient electromagnetic generator based on controlled rectifier," in *Proc. 25th Int. Conf. Elect. Machines Syst.*, 2022, pp. 1–6.

[21] G. Bertotti, F. Fiorillo, and G. Soardo, "Dependence of power losses on peak magnetization and magnetization frequency in grain-oriented and non-oriented 3% SiFe," *IEEE Trans. Magn.*, vol. 23, no. 5, pp. 3520–3522, Sep. 1987.

Guilu Min (Student Member, IEEE) received the B.S. degree in electrical engineering from Changzhou Institute of Technology, Changzhou, China, in 2022. She is currently working toward the Ph.D. degree in physical electronics with Nanjing Normal University, Nanjing, China.

Her research interests include the doubly salient machine control.

Yanwu Xu (Member, IEEE) received the B.S. degree in measurement engineering and the M.S. degree in automation engineering, both from Anhui University, Hefei, China, in 2012 and 2015, respectively, and the Ph.D. degree in electrical engineering from Nanjing University of Aeronautics and Astronautics, Nanjing, China, in 2020. From December 2019 to March 2020, he was a visiting Ph.D. student with the Stability & Optimization & Data-Analytics Group, Nanyang Technological University, Singapore. Since 2020, he has been a Member of the Faculty with the School of Electrical and Automation Engineering, Nanjing Normal University, where he is currently an Associate Professor. His research interests include the doubly salient electric machine design and control, the electrical power generation and the micro-grid for the more electric aircraft.

Shuye Ding was born in 1978. He received the B.S., M.S., and Ph.D. degrees in electrical machinery and appliance from Harbin University of Science and Technology, Harbin, China, in 2001, 2004, and 2008, respectively.

He is currently a Professor with the School of Electrical and Automation Engineering, Nanjing Normal University, Nanjing, China. He is the author or coauthor of more than 80 published peer-reviewed papers and holds more than 10 patents. His research interests include synthesis physical fields of large electrical machines and theoretical study of special electrical machines.

Zhuoran Zhang (Senior Member, IEEE) received the B.S. degree in measurement engineering and the M.S. and Ph.D. degrees in electrical engineering from Nanjing University of Aeronautics and Astronautics (NUAA), Nanjing, China, in 2000, 2003, and 2009, respectively.

Since 2003, he has been a Member of the Faculty with the Department of Electrical Engineering, NUAA, where he is currently a Full Professor and the Dean of the College of Civil Aviation. From February 2012 to June 2013, he was a Visiting Professor with Wisconsin Electric Machines and Power Electronics Consortium (WEMPEC), University of Wisconsin-Madison, Madison, WI, USA. He has authored or coauthored over 230 technical papers and two books and is the holder of 70 issued patents in these areas. His research interests include electrical machines and drives with emphasis on permanent magnet machines, hybrid excitation electric machines, and doubly salient electric machines for aircraft power, electric vehicles, and renewable energy generation.

Dr. Zhang was the recipient of the Best Paper Awards from IEEE Vehicle Power and Propulsion Conference 2013, 2018 International Conference on Electrical Machines and System, 2023 International Conference on Electrical Machines and System and 2024 International Conference on Electrical Machines.